LA-UR-16-25986
Approved for public release; distribution is unlimited.

Title: Design of the Next Generation Target at the Lujan Neutron Scattering Center, LANSCE.

Author(s): Ferres, Laurent

Intended for: Report

Issued: 2016-08-03

Design of the Next Generation Target at the Lujan Neutron Scattering Center, LANSCE.

Second year of engineering school, internship

- FERRES Laurent
- 2A - Electronic and applied physics, Major nuclear engineering
- university year 2015/2016
- lab advisor: NOWICKI Suzanne
- ENSICAEN advisor : GUILLON Benoit

ACKNOWLEDGEMENTS

I WOULD LIKE TO THANK :

-Aaron Couture (P-27 acting group leader) for giving me the opportunity to work at the Lujan Neutron Scattering Center,

-MICHAEL MOCKO (SUPERVISOR) FOR THE GREAT DISCUSSIONS AND SUPPORT THROUGHOUT THIS WORK

-STEPHEN WENDER (HOST) FOR HIS KNOWLEDGE AND HELP DURING MY WORK

-SUZANNE NOWICKI (MENTOR) FOR OFFERING ME THIS INTERNSHIP AND MENTORING ME DURING THIS THREE-MONTH PERIOD

Table of Contents

I. INTRODUCTION

1. The Laboratory

Los Alamos National Laboratory (LANL) [a] supports scientific research in many diverse fields such as biology, chemistry, and nuclear science. The Laboratory was established in 1943 during the Second World War to develop nuclear weapons. Today, LANL is one of the largest laboratories dedicated to nuclear defense and operates an 800 MeV proton linear accelerator for basic and applied research including: production of high- and low-energy neutrons beams, isotope production for medical applications and proton radiography. This accelerator is located at the Los Alamos Neutron Science Center (LANSCE). The work performed involved the redesign of the target for the low-energy neutron source at the Lujan Neutron Scattering Center, which is one of the facilities built around the accelerator.

The redesign of the target involves modeling various arrangements of the moderator-reflector-shield for the next generation neutron production target. This is done using Monte Carlo N-Particle eXtended (MCNPX), and ROOT analysis framework, a C++ based-software, to analyze the results.

2. Context

The LANSCE facility employs a 1-MW linear proton accelerator (LINAC), which generates an 800 MeV proton beam. A part of this beam goes to the Lujan Neutron Scattering center and impinges onto a tungsten target to generate spallation neutrons. These neutrons are further slowed down and thermalized in moderators (the assembly is called Target-Moderator-Reflector-Shield (TMRS), Fig. 1.). These thermal and cold neutrons are then available in 16 neutron Flight Paths (FPs).

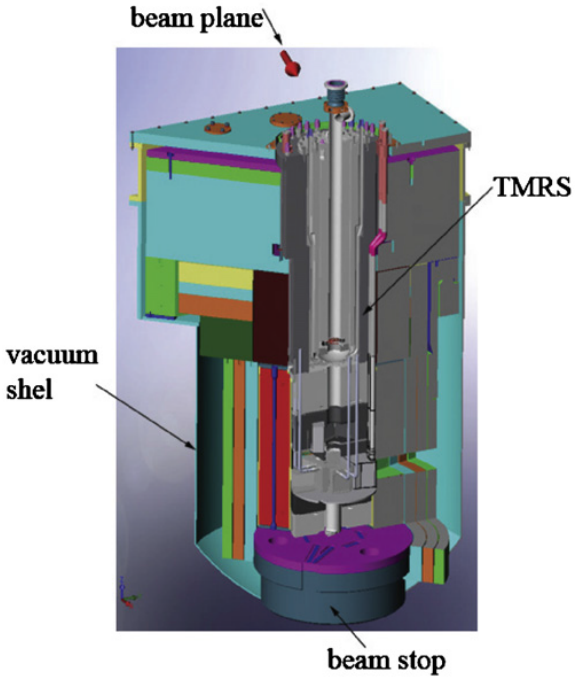

Figure 1. TMRS scheme

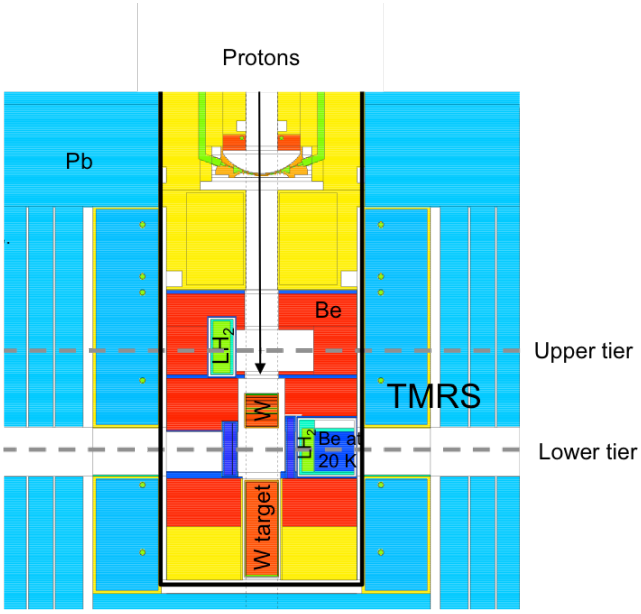

Figure 2. MCPX Mark III target design

The Lujan TMRS has a rather compact cylindrical assembly that is approximately 3-m tall and 60 cm in diameter. This compact and cylindrical shape allows ample room for the crypt to fit into the assembly. The crypt is composed of a steal vessel that provides a vacuum shell which contains a steel reflector, shield, and a beam stop. 3 m of steel plate embedded in heavy concrete surrounding the entire apparatus [b].

The current target is known as Mark III (Fig. 2.) and is composed of two tungsten targets : one upper target of 9.1 cm thickness located between the upper and lower-tier moderators, and one lower target of 29.8 cm thickness placed below the lower-tier moderators. Both are 10 cm in diameter and the gap between them is 18.4 cm. The upper target is composed of 7 plates, each one being separated by water, used to cool the tungsten [b, c].

The neutron moderators are arranged in two tiers with a vertical orientation : upper and lower tier as shown in Fig. 2. Four FPs are viewing the moderators located in the upper tier and 12 in the lower tier. A variety of neutron scattering instruments are placed at different FPs utilizing the available thermal or cold neutrons. The instruments suite at Lujan Center supports a great variety of scientific disciplines : materials science, physics, chemistry, and biology.

The moderators are water and liquid hydrogen in the lower tier and in the upper tier. There is a beryllium reflector to focus the beam in the FPs, and the outer shield is lead.

3. Motivation

A model based on the previous Mark III model was studied [b, c], where the upper target is translated in the field of view of the upper tier in such a way that the gap between the two targets is changed to 37.5 cm. The upper reflector and moderator have been removed. As seen in Fig. 3, the neutrons that came out from the outer surface of the upper tungsten target were directly in the energy range desired. Table 1 shows how the several energy ranges are divided.

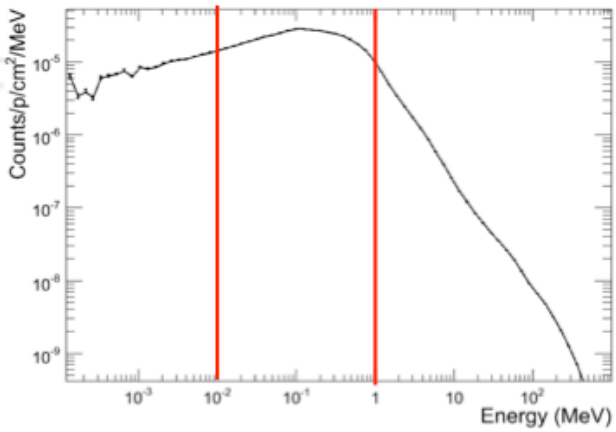

Figure 3. Neutron spectrum at the outer surface of the upper target

Table 1. Energy ranges

	Energy ranges
Cold neutrons	<5 meV
Thermal neutrons	5 meV - 0.4 eV
Low energy range	0.4 eV – 100 eV
Epithermal energy range	100 eV – 10keV
Medium energy range	10 keV – 1 MeV
Fast energy range	1 – 100 MeV

Although we are able to increase the flux in the epithermal and medium energy ranges in the upper tier by translating the target, the thermal neutron flux decreases by a factor of two in the lower tier.

The purpose of these studies is to understand how the upper target contributes to the neutron flux in both the upper and lower tier.

II. SIMULATIONS AND RESULTS

1. Simple designs

To increase efficiency in our calculations, we modeled several simple designs of the 2-piece tungsten target in order to understand the characteristics of the proton and neutron fluxes on the outer, upper, and lower surfaces of the upper and lower tungsten targets. The

simple models were built using Monte Carlo N particle eXtended (MCNPX) in the configuration described below.

a) Proton beam studies

(i) Model

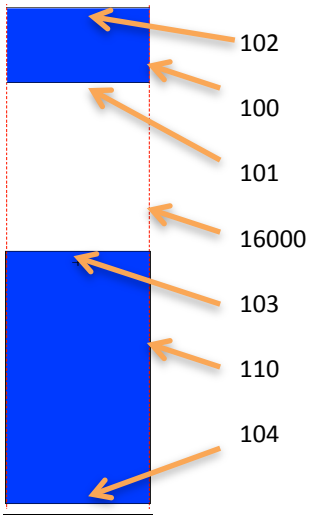

Figure 4. **Simple model**

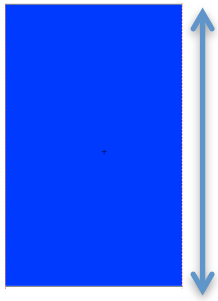

Figure 5. Thickness variation of the upper target

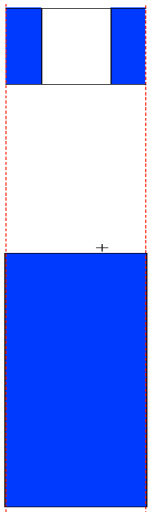

Figure 6. Hole in the upper target

Figure 4 shows the upper and lower tungsten targets. They are both cylindrical with lengths of 9 cm and 30 cm for the upper and lower target respectively, and a diameter of 10 cm. The space between the two targets is roughly 20 cm. For simplicity, we did not include the plates of water, the Inconel enclosures that can be found in the current Mark III design. In this model, the upper surface, the lower surface, and the outer surface of the upper target are labeled as 102, 101 and 100, respectively. The upper surface, the lower surface, and the outer surface of the lower target are labeled 103, 104 and 110, respectively. The monoenergetic 800 MeV proton beam is perpendicular to surface 102 of the upper target and follows a Gaussian distribution with a full width half maximum (FWHM) of roughly 3.5 cm and 99 % of the protons are contained within a 10 cm diameter cylinder. Therefore, all the protons hit the upper tungsten target.

First, a simulation was made where the thickness of the upper target varies from 0.5 to 35 cm as can be seen in Fig. 5. The goal of this simulation was to characterize the intensity and the energy distribution of the proton flux on the outer surfaces of the upper target as a function of the thickness of the tungsten target.

Then, in order to regain some of the lost neutrons in the lower tier as explained in the introduction section, a simulation was made with a hole in the upper target with a diameter that varies from 0.5 to 9 cm as shown in Fig. 6. The goal was to see if more neutrons in the lower target can be created by having the beam of 800 MeV go through the upper target.

(ii) Results

We first report the results for the proton study. We used a F2 tally on surface 103 and we used the ROOT analysis framework to plot the intensity of the protons as a function of the energy. We call it the proton spectrum.

a) Thickness study

Figure 7 shows the proton spectrum as a function of the thickness of the upper target. We can observe that as the thickness increases, the average energy of the protons that emerge from the upper target decreases.

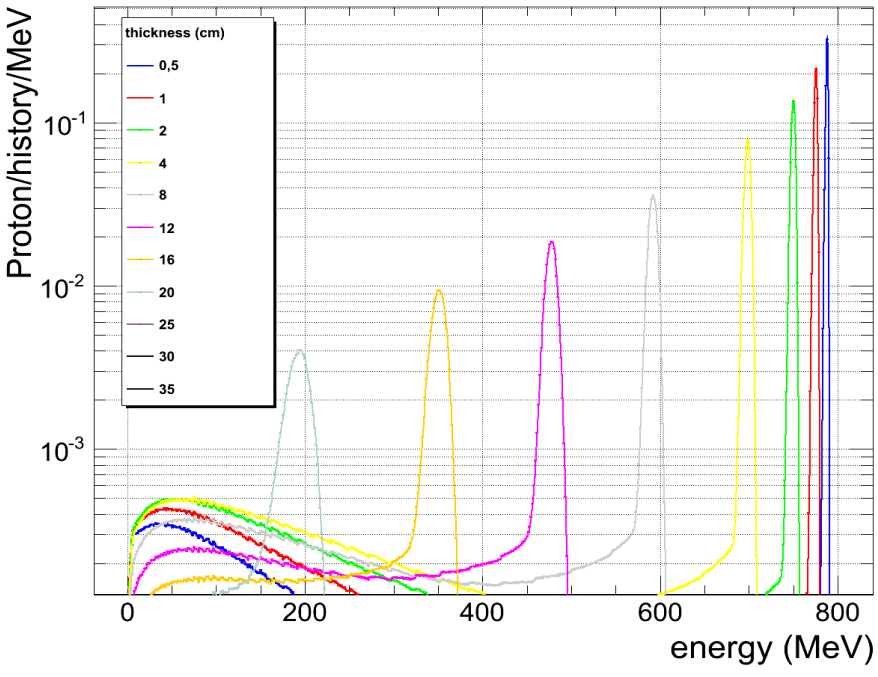

Figure 7. Proton spectrum as a function of upper target thickness.

Figure 8 reports the centroid of the peak and the average energy of the distribution as a function of thickness. The first thing to note is that when the upper target thickness is 8.7 cm (similar to Mark III), the average energy of the protons is 570 MeV when they

exit the upper target (at surface 101). The average energy is lower than the centroid of the peak because the curve extends beyond the primary area of proton intensity at that energy.

We can see that above 20 cm we do not report the peak centroid and the average energy. This is because all the protons have been absorbed by the tungsten when the thickness is above 20 cm. Considering the fact that in Mark III, the upper target is about 8.7 cm and the lower target is about 30 cm, we can say that all the protons are absorbed. Thus, the purpose of these studies is not to find a way to create more neutrons, but to find a way to shift the energy of the neutrons in the range of interest for the upper and the lower target.

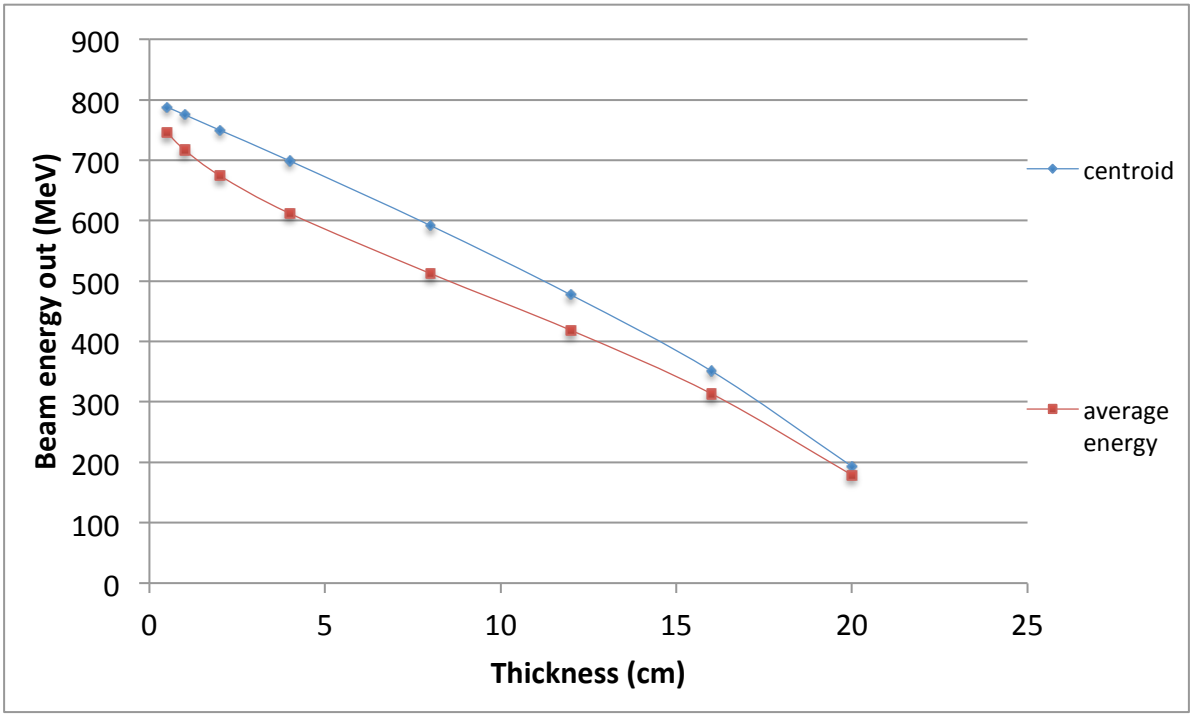

Figure 8. Peak centroid and average energy of the protons on the lower surface of the target as a function of thickness

b) Hole study

Figure 9 shows the intensity of the protons as a function of the energy on the upper surface of the lower target (103) when there is a hole in the upper target. The results show that as we increase the diameter of the hole, we increase the neutron production in the lower tier at the expense of the neutron production in the upper tier. In this model, we kept the thickness of the upper target at 8.7 cm, which is similar to Mark III. We can observe two

peaks : one at 570 MeV and another one at 800 MeV. This is directly a result from the protons that lose on average 230 MeV when going through 8.7 cm of tungsten, but do not lose any energy when going through the hole.

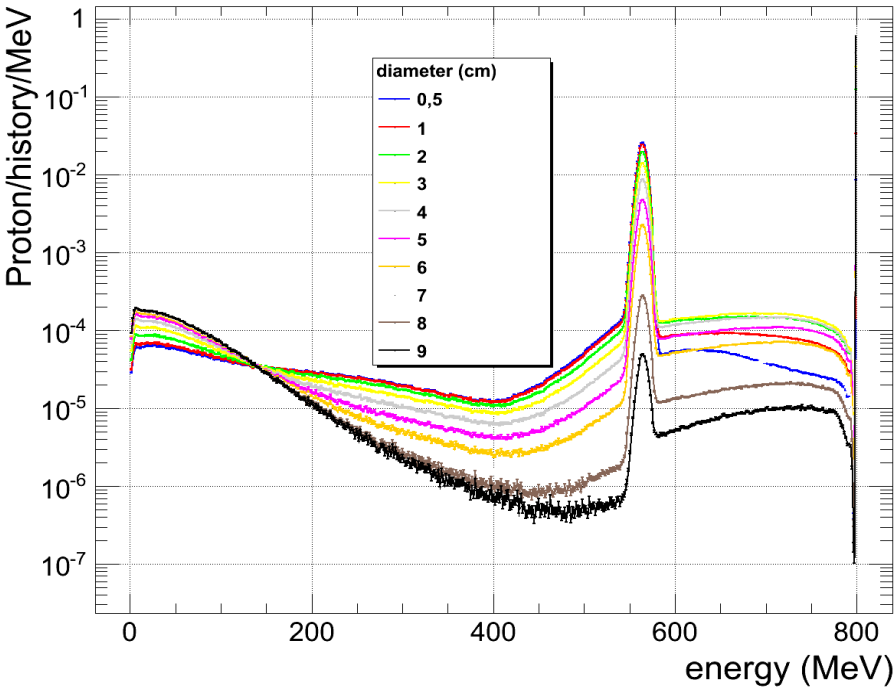

Figure 9. Proton spectrum as a function of hole diameter in the upper target

b) Neutrons studies

Although simulation allows us to make a hole in the upper target easily, the reality is very different. In fact, to mechanically design the upper target with a hole in the middle can be challenging. Therefore, we decided that it would be easier to decrease the radius of the upper target and let the 800 MeV protons go through that way. We present here the neutron study when we vary the diameter of the upper target.

(i) Model

In this study, the upper target diameter ranges from 1 to 10 cm as seen in Figure 10.

Figure 10. Diameter variation in the upper target

The purpose of these studies was to characterize the neutron beam, its spectrum, and intensity on the outer surface.

(ii) Results

Figure 11 shows the neutron spectrum on the outer surface of the upper target as a function of the diameter of the upper target. We can see that, as expected, there are more neutrons that are produced as we increase the diameter of the upper target. However, the shape remains about the same. The intensity peaks between 0.1 and 1 MeV independently of the diameter variation.

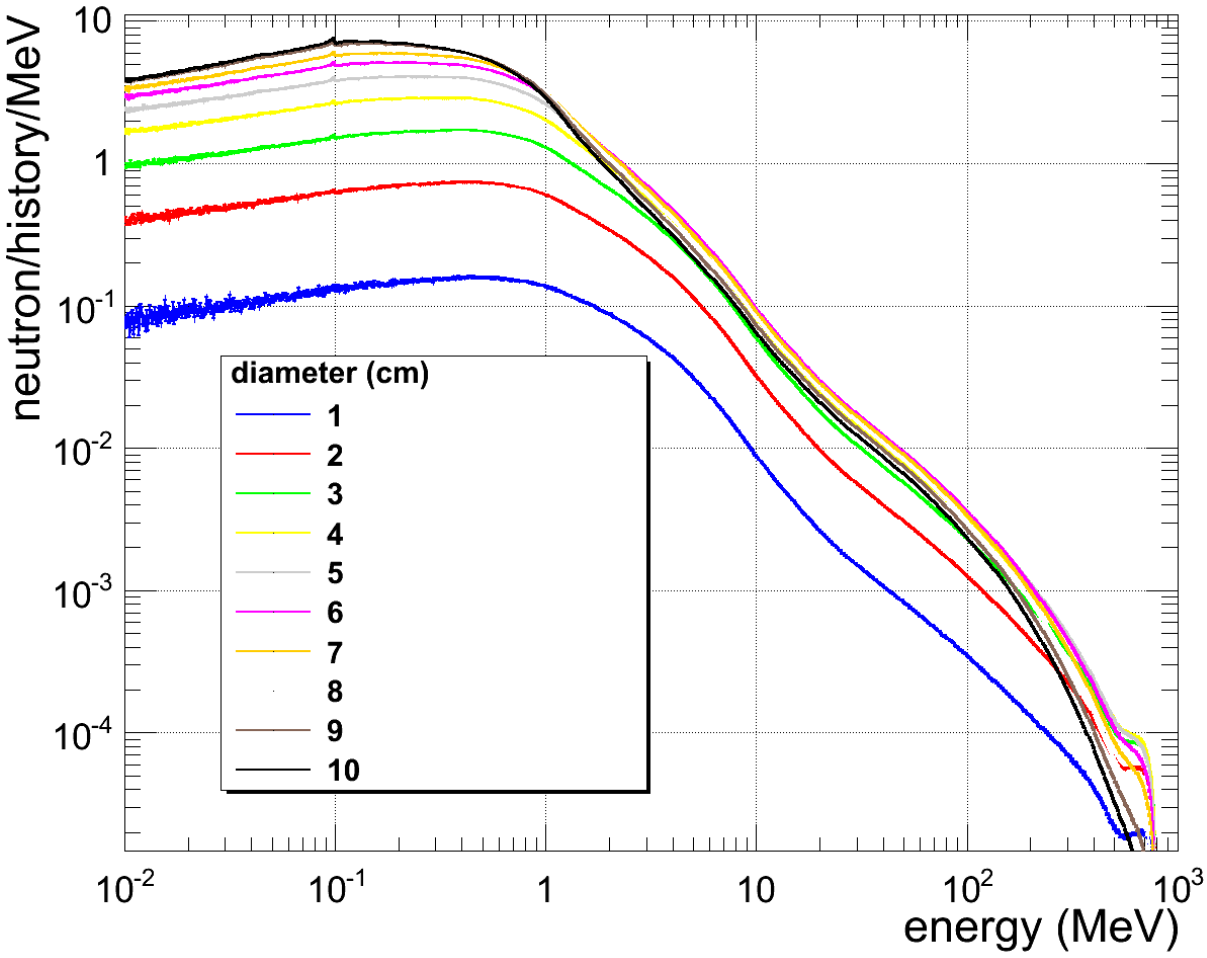

Figure 11. Neutron spectrum on the outer surface of the upper target

Figures 12 and 13 show the intensity on the outer surface of the upper and lower targets as a function of the diameter for the hole model and the anti-hole model.

We can see as expected that when the hole widens, the neutron production in the upper tier decreases as the neutron production in the lower tier increases. Also, if we sum the neutron contribution from all surfaces, it remains constant at less than 2%, which shows that the neutron production remains the same. This is similar to the “anti-hole” model. We also

notice that above roughly 7 cm the number of neutrons that are produced at the outer surface of the upper and lower target remains about constant in both cases. This is a simple manifestation of a Gaussian beam profile, so 70% of the protons are in a 5 cm diameter cylinder, at the middle of the beam. Another thing is that in the "anti-hole" study, at about a diameter of 7 cm, the production starts to decrease because the neutrons are stopped in the tungsten without escaping.

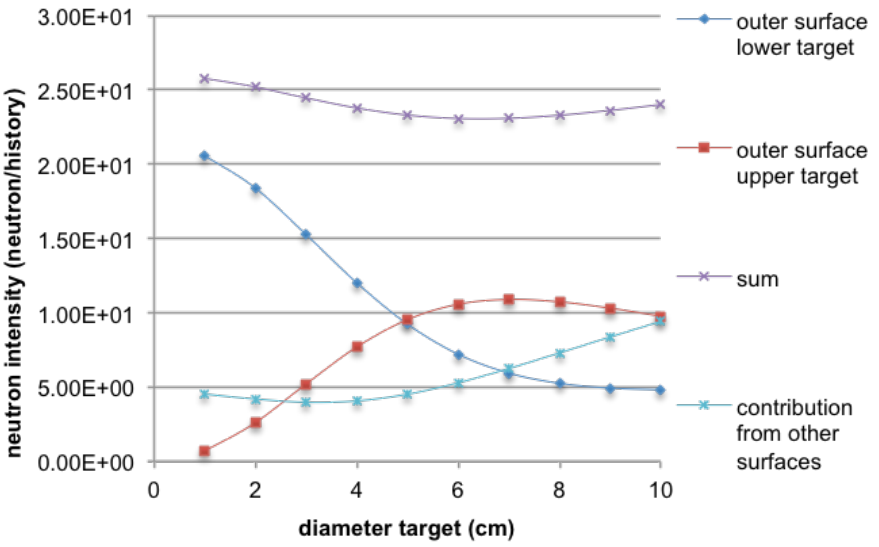

Figure 12. Neutron intensity in the lower and upper tier, anti-hole model

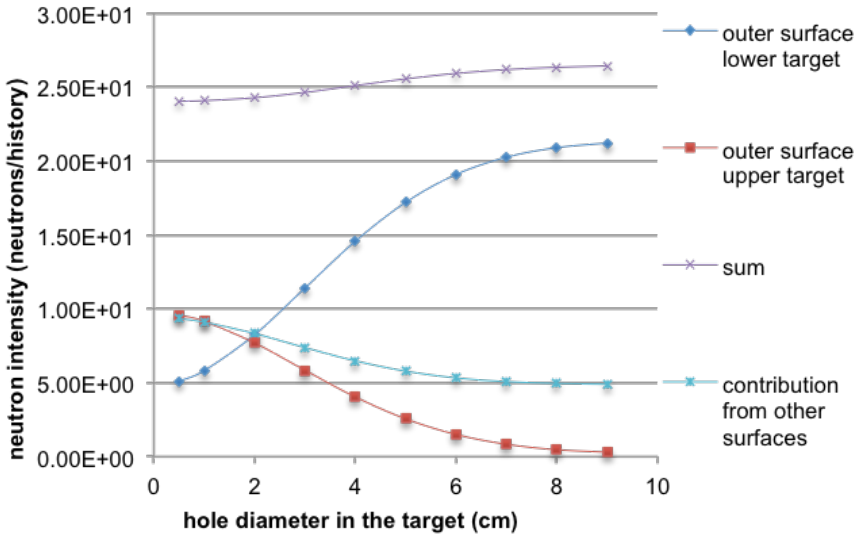

Figure 13. Neutron intensity in the lower and upper tier, hole model

2. Realistic designs

The hole and "anti-hole" models were then simulated with a complex geometry as we described in the introduction. As seen in the figures below, the MCNPX complex geometry primarily includes :

1) the plates of water in the upper target (used for cooling),

2) the Inconel for the upper and lower target,

3) the moderators and Be reflectors in the lower tier

4) the Pb outer reflector

In this model, there is 9.1 cm of tungsten in the upper target and 29.8 cm of tungsten in the lower. The space between the two targets is 35.5 cm.

In these simulations, an F5 tally was used to study the intensity and the spectrum of the neutrons at the end of the FPs in the upper and lower tiers.

a) Hole in the upper target

(i) Model

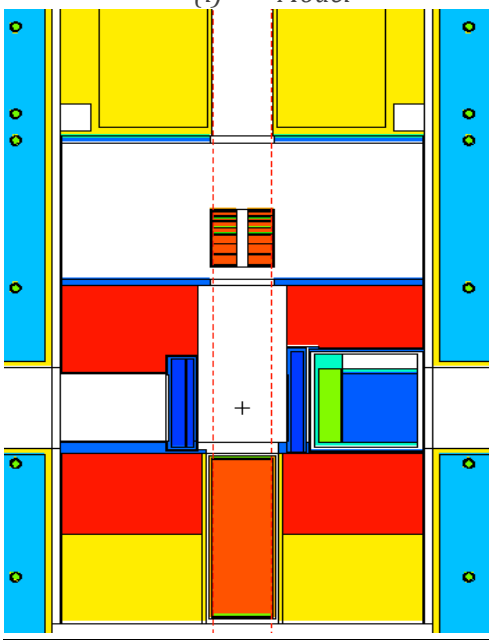

Figure 14. Translated target with a hole in the upper target MCNPX design

A hole was implemented in the upper target (Fig. 14.) and 9 simulations were done with a diameter ranging from 1 to 9 cm. In those conditions, as seen in the simple model section above, the number of thermal neutrons in the lower tier increases as some of the 800 MeV protons hit the lower target.

(ii) Results

As explained in the introduction, the purpose of these simulations is to study the production of epithermal and medium-energy neutrons in the upper tier as a function of the thermal neutrons in the lower tier.

Figures 15 and 16 show the neutron spectrum in the lower and upper tier for the hole model described above. We compare all the results to Mark III and the translated target model :

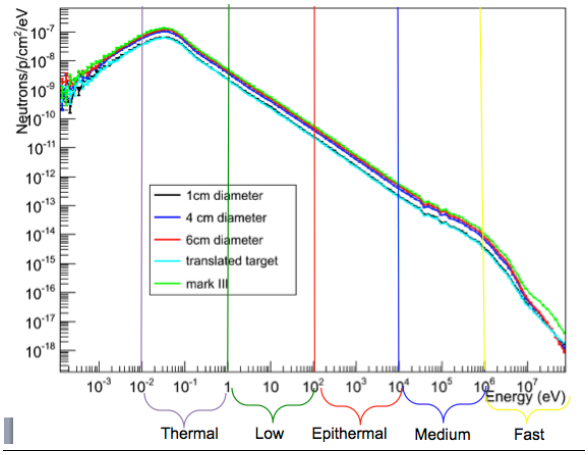

Figure 15. Neutron spectrum in the lower tier

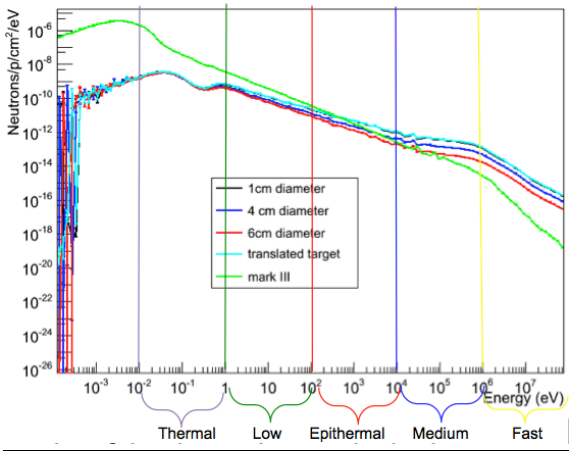

Figure 14. Neutron spectrum in upper tier

These figures highlight the different energy ranges. Figure 17 and 18 show the integral of the neutron spectrum presented in Figures 15 and 16 for each energy range, respectively.

Due to the tally used, the ordinate is presented in neutrons/protons/cm^2/eV. Thus, it is not possible to fully realize the neutron intensity of each range just by looking at the spectrum. The following bar charts result from the calculation of the integral below the curves.

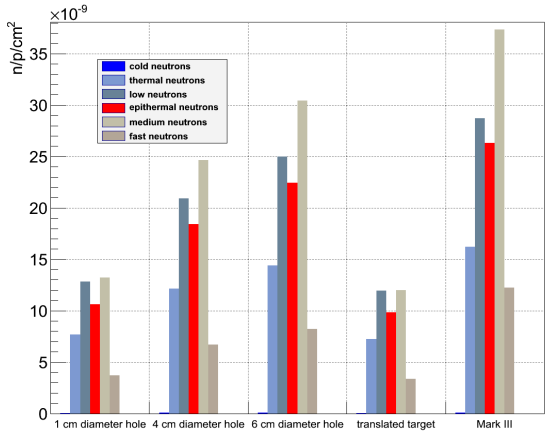

Figure 17. Neutron intensity in the lower tier

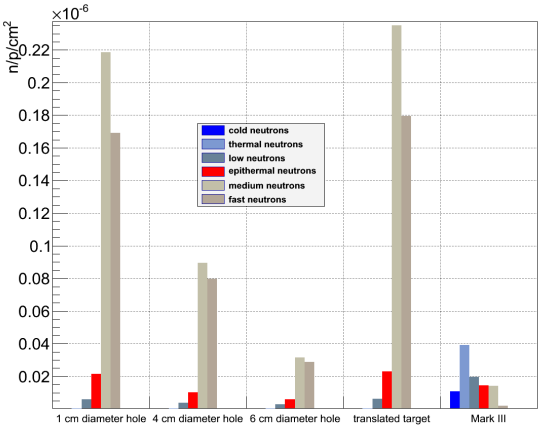

Figure 18. Neutron intensity in the upper tier

We notice that compared to Mark III, the 6 cm-diameter hole model has fewer thermal neutrons in the lower tier, but the ratio of thermal neutrons to fast neutrons is lower (0.57 fast neutron for 1 thermal neutron the 6 cm-diameter model instead of 0.75 fast neutron for 1 thermal neutron in the Mark III model).

Because time of flight measurements are used by researchers to accurately calculate the energy of the neutrons, it is important to keep the fast neutrons at a low rate in order to keep a high dynamic range. Fast neutrons can be thermalized when hitting the materials around the instruments and can be counted as a thermal neutron instead of a fast neutron. Therefore, the ratio of fast to thermal neutrons has to be kept as low as possible.

In the upper tier, the production of epithermal and fast neutrons (medium energy range) decreases rapidly when increasing the diameter of the hole, compared to the translated target model. Thus, the high-energy neutron production in the upper tier will decrease by a factor of 20 % if the diameter of the hole exceeds 2 cm.

b) Middle target design

(i) Model

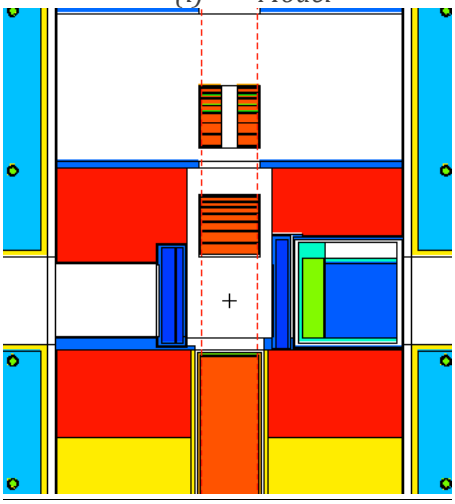

Figure 19. Translated target with a hole in the upper target and a target in the middle MCNPX design

Another concept is to add a target in the middle as seen in Fig. 19. This design is a combination between the translated target and the Mark III models. With this geometry, we hope to recover some of the thermal neutrons in the lower tier.

(ii) Results

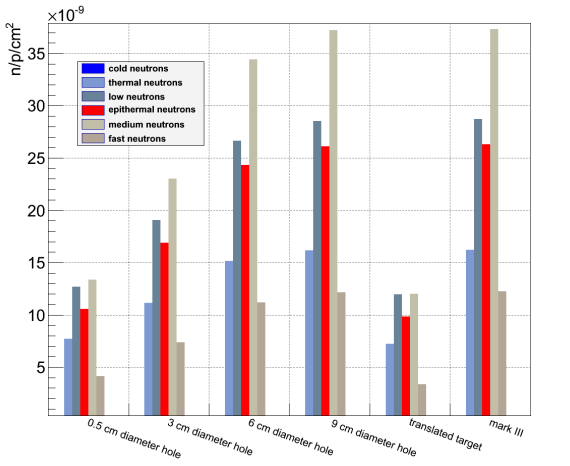

Figure 20. Neutron intensity in the lower tier

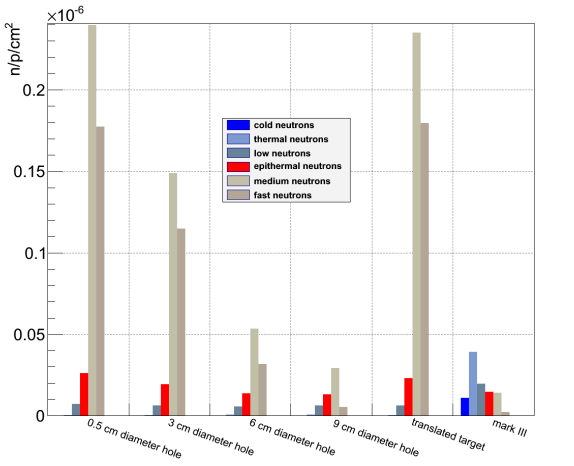

Figure 21. Neutron intensity in the upper tier

As expected, by adding tungsten material closer to the lower tier, the neutron production has increased. As seen in Fig. 20, when the hole is 9 cm in diameter, the integral for each energy range is about the same as in Mark III in the lower tier. However, the

epithermal and fast neutron production in the upper tier is similar to the translated target design (Fig. 21.) when the hole is very small.

c) "Anti-hole" design

(i) Model

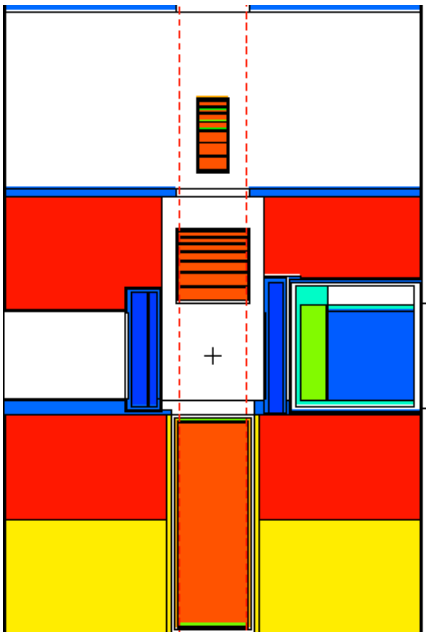

Figure 22. "Anti-hole" design

The proton beam is modeled with a Gaussian shape with a FWHM of 3.53 cm, which means that about 70 % of the flux is concentrated in a 5-cm cylinder. For that reason, when the diameter of the hole is greater than 5 cm, the flux does not change. Therefore, we decided to model an "anti-hole" design (Fig. 22).

(ii) Results

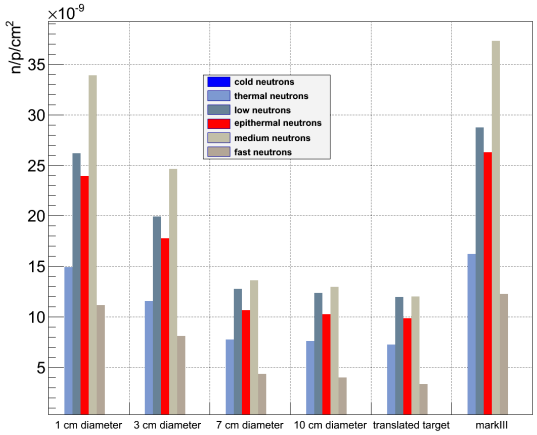

Figure 23. Neutron intensity in the lower tier

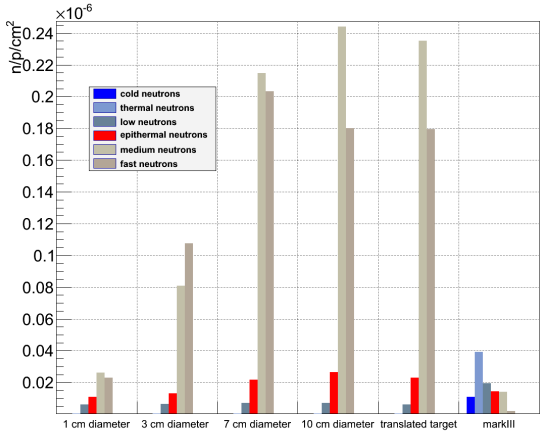

Figure 24. Neutron intensity in the upper tier

We observe that when the diameter of the upper target reaches 5 cm, the thermal neutron intensity in the lower tier does not change anymore (Fig 23. and 24.). However, there are less fast neutrons in the lower tier with a 10 cm diameter target compared with a 7 cm diameter target.

d) Filter study

(i) Model

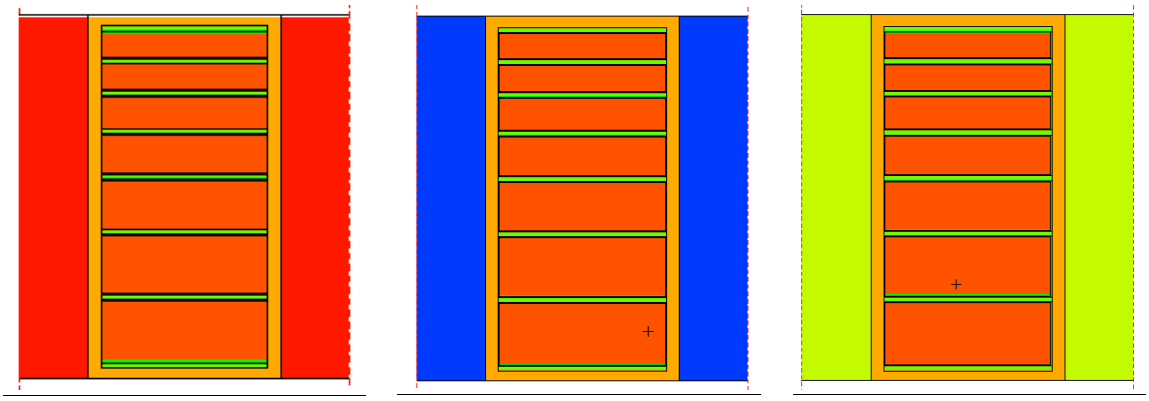

Figure 25. Be, H2O and D2O filter MCNPX design

The spectrum of neutrons coming out of the outer surface is much lower until the diameter reaches 5 cm. The spectrum then remains mostly constant until 7 cm compared to the simple model as shown in Fig. 9. Following these results, beryllium, deuterium, and

hydrogen filter have been added around the 5 cm diameter upper target to moderate fast neutrons coming out directly from the outer surface.

(ii) Results

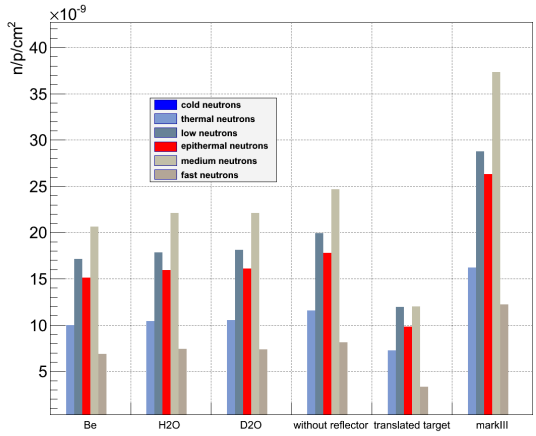

Figure 26. Neutron intensity in the lower tier

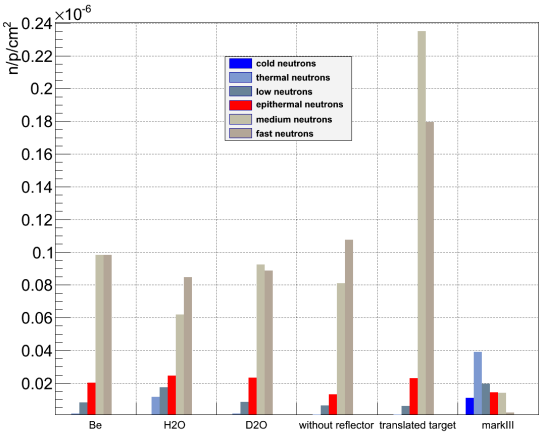

Figure 27. Neutron intensity in the upper tier

The intensity variation of the neutron energy ranges is not very important (less than 3%) in the lower tier (Fig. 26.), which is normal because in those 3 cases, the filter is composed of light material that allow protons to go through. However, according to Fig. 27, beryllium seems to work best in terms of high-energy neutron production.

e) Figure of merit

Figure 28 illustrates the intensity of the medium range energy neutrons in the upper tier versus the intensity of thermal neutrons in the lower tier. Following these results, it seems to be the “HoleAndMiddle” model (hole in the upper target and a target in the middle, at the Mark III upper target location) that presents the best compromise.

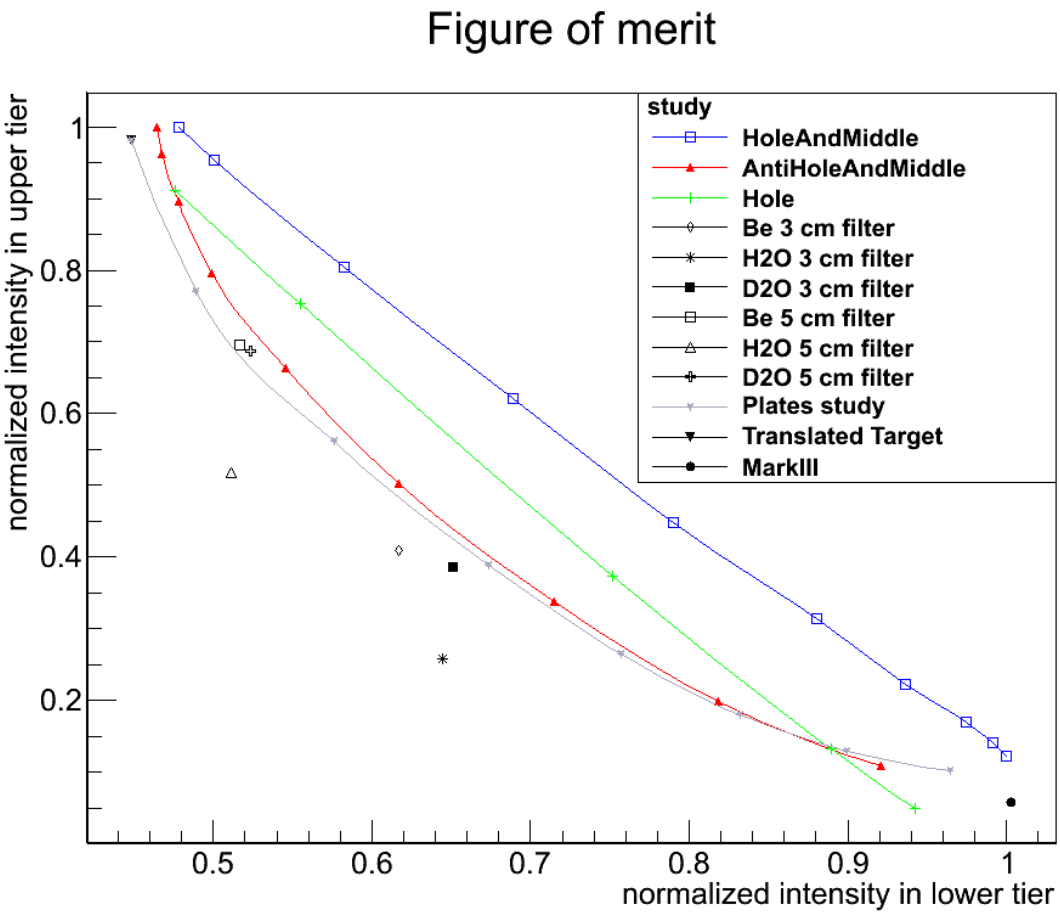

Figure 28. Figure of merit

III. CONCLUSION

The MCNPX simulations have shown that adding a middle target at the location of the current Mark III upper target (HoleAndMiddle, Fig. 29) provides the best compromise between the intensity of the medium range energy neutrons in the upper tier and the thermal neutrons in the lower tier. However, it can present a mechanical challenge to design the upper target with a hole in the middle.

We studied and characterized the neutron production behavior with several material/reflector/filter arrangements in the TMRS. In the future, we will study whether changing the field of view of the FPs could improve the neutron production as only about half of the upper target is currently in the field of view of the FPs. We will then determine if it is worthwhile creating new FPs for the next generation target.

IV. REFERENCES

a) Los Alamos National Lab website : http://www.lanl.gov/

b) M. Mocko, G. Muhrer, Fourth-generation spallation neutron target-moderator-reflector-shield assembly at the Manuel Lujan Jr. neutron scattering center, NIMA, Volume 704, 11 March 2013, Pages 27–35

c) S. Nowicki, M. Mocko, Design of the Fifth-Generation Target-Moderator-Reflector-Shield Assembly, Twelfth International Topical Meeting on Nuclear Applications of Accelerators (AccApp'15), 2015-11-10 (Washington DC, District Of Columbia, United States)

V. ANNEXES

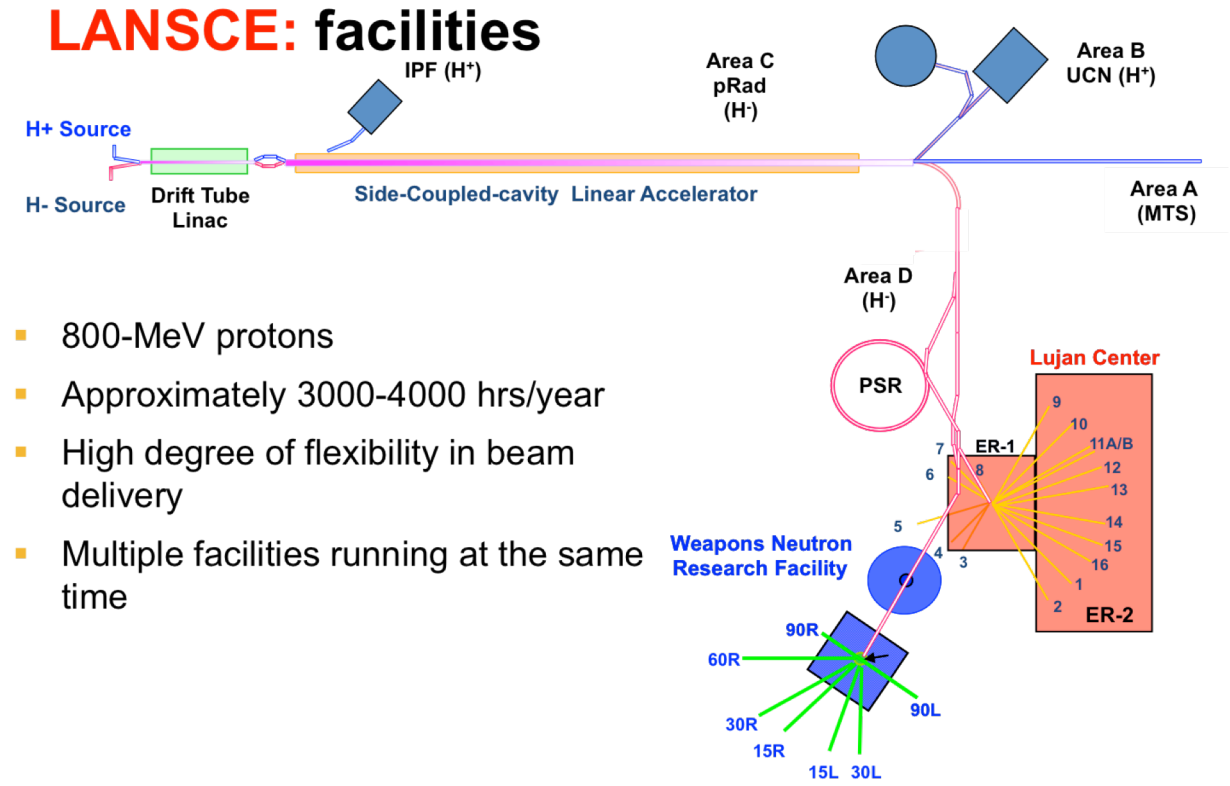

Figure 25. Scheme of the LANSCE accelerator facility

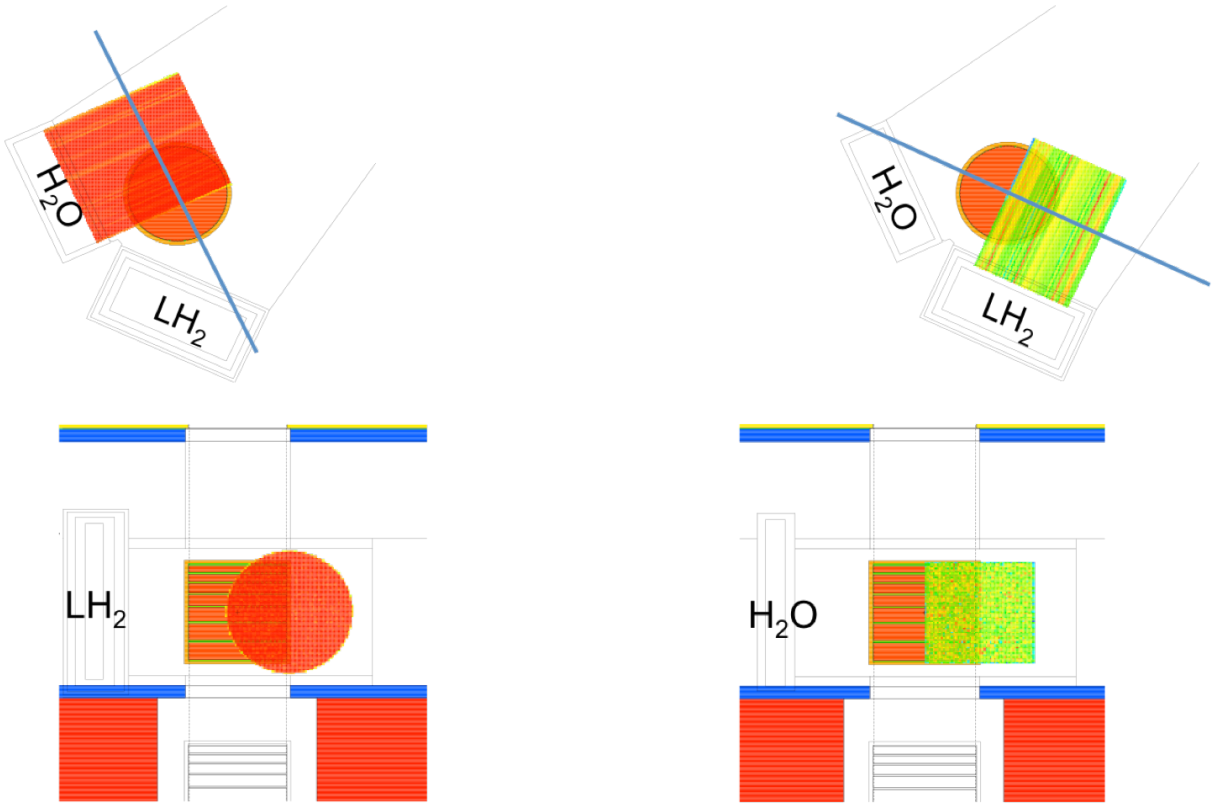

Figure 306. Field of view on the upper tier FPs. Left: FP15, right: FP12.

Here ais some of the ROOT code used to make some of the figures seen in this report :

In order to establish the barcharts, weh ad to calcul the integrals below the curve :

```
Double_t* CalculateIntegrals(Int_t index, Double_t emin, Double_t emax)
 {
  // Energy is in eV
  // cold neutrons: 1 meV - 5 meV
  Double_t ecold1=0.001;
  Double_t ecold2=0.005;
  // thermal range: 5 meV - 0.4 eV
  Double_t eth1=0.005;
  Double_t eth2=0.4;
  // low energy range: 0.4 eV - 100eV
  Double_t elow1=0.4;
  Double_t elow2=100;
  // epithermal energy range: 100 eV - 10 keV
  Double_t eepi1=100;
  Double_t eepi2=1E4;
  // medium energy range: 10 keV - 1 MeV
  Double_t emed1=1E4;
  Double_t emed2=1E6;
  // fast energy range: 1 MeV - 100 MeV
  Double_t efast1=1E6;
  Double_t efast2=1E8;

  //Int_t size = 6;
  //TArrayD I = new TArrayD(size);
  Double_t *I = new Double_t[6];

  TGraphErrors *g1 = GetSpectrum(index,"eV",-1,emin,emax);

I[0] = GetIntegral(g1,ecold1,ecold2);
I[1] = GetIntegral(g1,eth1,eth2);
I[2] = GetIntegral(g1,elow1,elow2);
I[3] = GetIntegral(g1,eepi1,eepi2);
I[4] = GetIntegral(g1,emed1,emed2);
I[5] = GetIntegral(g1,efast1,efast2);

/*cerr<< "\n";
cerr<< "**********************************\n";
cerr<< "Cold neutrons: 1 meV - 5 meV:\n";
cerr<< I[0];
cerr<<" n/p/cm2 \n ";

cerr<< "Thermal neutrons: 5 meV - 0.4 eV:\n";
cerr<< I[1];
cerr<<" n/p/cm2 \n ";

cerr<< "Low energy neutrons: 0.4 eV - 100 eV:\n";
cerr<< I[2];
cerr<<" n/p/cm2 \n ";

cerr<< "Epithermal neutrons: 100 eV - 10 keV:\n";
cerr<< I[3];
cerr<<" n/p/cm2 \n ";

cerr<< "Medium energy neutrons: 10 keV - 1 MeV:\n";
cerr<< I[4];
cerr<<" n/p/cm2 \n ";

cerr<< "Fast neutrons: 1 MeV - 100 MeV:\n";
cerr<< I[5];
cerr<<" n/p/cm2 \n ";*/

return I;
//delete[] I;
```

Root code used to create the barchart plots :

```
{

 gROOT->ProcessLine(".L /user/lferres/root_scripts/Functions.C");
 gROOT->ProcessLine(".L /user/lferres/root_scripts/Read.C");
 gROOT->ProcessLine(".L /user/lferres/root_scripts/PlotSpectrum.C");

 Int_t tallytype[2]={15, 125};
 Int_t i, j;

 // Energy is in eV
 Double_t emin=0.0001;
 Double_t emax=1E8;

 //Number of plates to move:
 const Int_t nx = 6;

 for (i=0; i<2; i++)
  {

    cerr<< "\n";
    cerr<< "*********************************\n";
    cerr<< "**************Tally ";T
    cerr<< tallytype[i];
    cerr<< "************\n";
    cerr<< "*********************************\n";

    ReadTallyF5("o0060.o", tallytype[i], 100, 1, 1); // without hole
    ReadTallyF5("o0061.o", tallytype[i], 101, 1, 1); // hole 1 cm diameter
    ReadTallyF5("o0062.o", tallytype[i], 102, 1, 1); // hole 2 cm diameter
    ReadTallyF5("o0064.o", tallytype[i], 103, 1, 1); // hole 4 cm diameter
    ReadTallyF5("o0066.o", tallytype[i], 104, 1, 1); // hole 6 cm diameter
    ReadTallyF5("o0068.o", tallytype[i], 105, 1, 1); // hole 8 cm diameter
    cout << "made it!" << "\n" ;


    Double_t* I=CalculateIntegrals(100, emin, emax);
    Double_t* J=CalculateIntegrals(101, emin, emax);
    Double_t* K=CalculateIntegrals(102, emin, emax);
    Double_t* L=CalculateIntegrals(103, emin, emax);
    Double_t* M=CalculateIntegrals(104, emin, emax);
    Double_t* N=CalculateIntegrals(105, emin, emax);

    if (i==0){
            float thermal[nx] = {I[1], J[1], K[1], L[1], M[1],N[1]};}
    if (i==1){
    float med[nx] = {I[4], J[4], K[4], L[4], M[4],N[1]};}

   /* if (i==0){
            float thermal[nx] = {I[1]/N[1], J[1]/N[1], K[1]/N[1], L[1]/N[1], M[1]/N[1],N[1]/N[1]};}
    if (i==1){
    float med[nx] = {I[4]/I[4], J[4]/I[4], K[4]/I[4], L[4]/I[4], M[4]/I[4],N[4]/I[4]};}*/

  }

 TCanvas *c1 = new TCanvas("c1","Figure Of Merit",200,10,1000,800);

 TGraph *gr = new TGraph(nx,thermal,med);
 gr->SetTitle("Figure of merit");
 //gr->GetXaxis()->SetTitle("normalized intensity in lower tier");
 //gr->GetYaxis()->SetTitle("normalized intensity in upper tier");
 gr->GetXaxis()->SetTitle("n/p/cm^{2} (FP-1 thermal range)");
 gr->GetYaxis()->SetTitle("n/p/cm^{2} (FP-12 medium range)");
 gr->Draw("AL*");
 return c1;

 //return;

}
```